



OPEN

Sensing the dynamics of oxidative stress using enhanced absorption in protein-loaded random media

SUBJECT AREAS:
MOLECULAR BIOLOGY
BIOLOGICAL TECHNIQUES
SENSORS AND PROBES
CELL SIGNALLINGGuillaume Suárez^{1*}, Christian Santschi^{1*}, Vera I. Slaveykova² & Olivier J. F. Martin¹Received
15 May 2013Accepted
15 November 2013Published
9 December 2013Correspondence and
requests for materials
should be addressed to
C.S. (christian.
santschi@epfl.ch) or
O.J.F.M. (olivier.
martin@epfl.ch)* These authors
contributed equally to
this work.¹Nanophotonics and Metrology Laboratory, Swiss Federal Institute of Technology Lausanne (EPFL), EPFL-STI-NAM, Station 11, CH-1015 Lausanne, Switzerland, ²Institute F. A. Forel, Earth and Environmental Sciences, Faculty of Sciences, University of Geneva, Route de Suisse 10, CH-1290 Versoix, Switzerland.

Reactive oxygen species play a key role in cell signalling and oxidative stress mechanisms, therefore, sensing their production by living organisms is of fundamental interest. Here we describe a novel biosensing method for extracellular detection of endogenous hydrogen peroxide (H₂O₂). The method is based on the enhancement of the optical absorption spectrum of the hemoprotein cytochrome *c* when loaded into a highly scattering random medium. Such a configuration enables, in contrast to existing techniques, non-invasive and dynamic detection of the oxidation of cyt *c* in the presence of H₂O₂ with unprecedented sensitivity. Dynamic information on the modification of the cell oxidative status of *Chlamydomonas reinhardtii*, an aquatic green algae, was obtained under oxidative stress conditions induced by the presence of trace concentrations of Cd(II). Furthermore, the dynamics of H₂O₂ production was investigated under different lighting conditions confirming the impact of Cd(II) on the photosynthetic activity of those phytoplanktonic cells.

The critical role that H₂O₂ and other reactive oxygen species (ROS) play in cell physiology is complex and multifaceted. ROS production is involved in cell signalling and in oxidative stress mechanisms that can lead to lipidic/nucleic peroxidation and cell death^{1–4}. Therefore, in parallel to the system biology perspective supported by genomics, proteomics and metabolomics, the development of analytical methods providing information on the dynamics of ROS generation is essential to gain further insights into the complex physiological processes of living cells and their response to environmental stress⁵. End-point bioassays based on membrane-permeable fluorescent and chemiluminescent probes are currently the most widely used techniques to measure oxidative stress and ROS production in biological cells exposed to different sources of stress^{6,7}. In addition, the spin-trapping electron spin resonance technique enables real-time probing of intra- and extracellular free radical ROS via the formation of semi-stable paramagnetic compounds⁸. However, such sensing methods based on free probe analysis are invasive and characterized by a series of drawbacks such as probe cytotoxicity or fluorescent dyes photobleaching. Electrochemical biosensors, with published detection limits of about tens of nanomolars are, on the other hand, a promising alternative offering non-invasive tracking of the ROS released from cell compartments⁹. Recently, Jin *et al.* used fluorescent single-wall carbon nanotube arrays to detect H₂O₂ at the micromolar range involved in signalling of epidermal growth factor receptors on the membrane of human carcinoma cells¹⁰.

The method presented here enables real-time measurements of H₂O₂ in the sub-nanomolar range. It relies on the ultra-sensitive optical detection of the redox state of cytochrome *c* (cyt *c*) loaded into a random medium in which the incident light undergoes multiple scattering similar to many naturally occurring optical phenomena including, for example, the blue colour of the sky, the iridescence of clouds and the broadband reflexion of white paint¹¹. Recently, multiple light scattering arrangements have been studied in the context of random lasers, where the gain medium supports multiple scattering¹². Replacing the gain medium by an absorbing medium has led to applications in fields such as photovoltaics¹³ and gas sensing¹⁴. Imaging of biological tissues represents a further application where multiple scattering comes into play¹⁵. Light passing through random media is subject to multiple scattering due to spatial variations of the refractive index. This prevents light from taking the shortest trajectory through the media and, consequently, the optical path through such type of media is increased. Multiple scattering in random or porous media has been investigated using analytical approaches based on Maxwell's equations¹⁶ and transport theory^{17,18}. The average optical path length of random media has been



determined using probabilistic Monte Carlo simulations¹⁹. In the presented configuration, the increased optical interaction length (OIL) produced by multiple scattering dramatically enhances the measured absorption of cyt *c* embedded in an aggregate (random medium) made of polystyrene beads (PS) and thus enables highly sensitive H₂O₂ detection. To illustrate the utilization of this method under environmentally relevant experimental conditions, we study the dynamics of H₂O₂ release by green microalga *Chlamydomonas reinhardtii* exposed to nanomolar concentrations of Cd(II). This study is important in itself for the following reason: The photosynthetic micro-alga *C. reinhardtii* is a representative primary producer at the origin of the food chain in aquatic systems and highly relevant from an ecotoxicology perspective. In addition to its environmental importance, the completion of the *C. reinhardtii* genome project revealed this microorganism as a useful model to investigate molecular cellular processes²⁰. Cadmium is a widespread environmental toxicant known to cause adverse effects in algae, including growth and chlorophyll synthesis inhibition^{21,22}, increase in the superoxide dismutase activity²³, phytochelatin induction²¹, and oxidative stress^{23,24}. *C. reinhardtii* homeostasis and tolerance to Cd(II) are well documented and the following chronological lethal sequence has been reported: oxidative stress, lipid and nucleic acid peroxidation, cell structure alteration, mutagenesis and apoptosis²⁵. However, most of the ecotoxicological studies examining the effects of Cd(II) contamination rely on acute stress conditions with Cd(II) concentrations in the hundreds of micromolar that strongly contrast with environmental concentrations, which are in the sub-micromolar range in freshwater²⁶. Recent studies have examined the intracellular ROS generation by flow cytometry²⁴ as well as the global expression profile of *C. reinhardtii*²³ under short term exposure conditions (typically a few hours) and environmentally relevant concentrations of Cd(II).

Results

Multiple light scattering enhances protein absorption in random media. Large enhancement of the OIL can be achieved by embedding absorbers, in this case cyt *c*, into a random medium¹⁴. As a consequence of the OIL lengthening through such a random medium, multiple scattering then dramatically enhances the spectroscopic information stemming from the cyt *c* redox state, as schematically illustrated in figure 1a. In this work we use aggregates of PS beads as random medium to enhance the absorption of cyt *c*, in order to lower the H₂O₂ detection limit. PS beads with a diameter of 0.94 μm and refractive index $n = 1.59$ are incorporated into a random matrix of cross-linked cyt *c* following the procedure detailed in the Methods section. Figure 1b shows a micrograph of the PS/cyt *c* aggregate recorded using focused ion beam microscopy, which clearly demonstrates the porous nature of the aggregate allowing rapid diffusion of H₂O₂ into the biosensor. The amplifying properties of the aggregate are characterised using Beer-Lambert's law. To this end, we compare serial, respectively parallel, dark-field configurations corresponding to the situations where scatterer and absorber are separated, respectively interspersed. In the serial configuration the same amount of cyt *c* as present in the PS/cyt *c* aggregate has been added to the top chamber separated by a thin glass cover slip from a control aggregate without cyt *c* placed in the bottom chamber. The aggregate was formed by cross-linking PS beads with bovine serum albumin (BSA) which exhibits a low absorbance within the wavelength range of interest, and can be used to define the zero absorption line I_0 used to determine the absorption. The molar absorbance coefficients of cyt *c* and BSA are shown in the supplementary figure 2. In the parallel configuration, the top chamber was filled with phosphate buffered saline (PBS) solution while the bottom chamber was occupied by the PS/cyt *c* aggregate. Once again, in order to compare both configurations, the number of cyt *c* located in the optical path was fixed (see "Methods online" for details). The

OIL ℓ for each configuration is then determined using Beer-Lambert's law, resulting in $\ell_s = 2$ mm and $\ell_p = 124$ mm for the serial and parallel configurations, respectively. The OIL for the serial configuration, ℓ_g , can also be calculated from the geometry of the sample chamber containing cyt *c* and the buffer solution, resulting in $\ell_g = 2$ mm which is in excellent agreement with the value obtained using Beer-Lambert's law. Thus, adding the random medium corresponds to a virtual increase of the OIL by a factor of 62 which increases the absorption signal by a factor of $v_A = 40$ for a cyt *c* concentration of 2 μM (Fig. 1b). The OIL were determined for $\lambda = 556$ nm, since the cyt *c* absorbance does not depend on the oxidation state at this wavelength (Supplementary Fig. 2).

Cyt *c* absorption enhancement enables ultrasensitive H₂O₂ detection. Cyt *c* exhibits different absorption peaks in its oxidised, respectively reduced state: a broad peak at $\lambda = 530$ nm, respectively narrower peaks at $\lambda = 520$ and $\lambda = 550$ nm (Supplementary Fig. 2). The redox catalytic activity of cyt *c*, the pseudo-peroxidase behaviour, in which the ferrous Fe^{II} heme group is oxidised into the ferric Fe^{III} heme group leading to H₂O₂ reduction into water, provides the spectroscopic information exploited here (Fig. 2a). The temporal evolution of the absorption spectrum of cyt *c* embedded into the PS/cyt *c* aggregate is measured using an inverted microscope in dark field configuration (Fig. 1c). Such a configuration efficiently suppresses the background level, producing a much better signal-to-background ratio (in the bright field configuration no measurable signal is detected, Supplementary Fig. 1). Thanks to multiple light scattering occurring in the PS/cyt *c* aggregate and the consecutive amplification of the absorption signal, the oxidation of tiny amounts of cyt *c* (typically 20 pmol) in the presence of H₂O₂ becomes measurable. The ability of the detection system to respond to H₂O₂ enzymatically produced in the sensing chamber was evaluated in the following experiment. The introduction of xanthine oxidase (XO) in the sensing chamber containing hypoxanthine (XH) and superoxide dismutase (SOD) catalytically generates superoxide anions which are then converted into H₂O₂. The obtained biosensor response curve (Supplementary Fig. 4) clearly indicates that the detection system is well suited for the real-time monitoring of released H₂O₂.

Calculation of a normalized redox state coefficient ϕ . The measured raw optical signal depends on the specific experimental conditions, in particular the geometry of the PS/cyt *c* aggregate. In order to obtain reproducible quantitative data, each raw cyt *c* spectrum is converted into a normalized oxidation state coefficient ϕ following the data analysis procedure detailed in the supplementary information (Supplementary Fig. 4). ϕ corresponds to the average oxidation state of cyt *c* present in the aggregate. It ranges between 0 and 1 for fully oxidized, respectively fully reduced samples, and does not depend on the signal background (Supplementary Fig. 3). The H₂O₂ concentration in the surrounding media can be derived via a calibration curve from the change of ϕ , $\Delta\phi$, defined as $\Delta\phi = \phi([H_2O_2]_{t=0}) - \phi([H_2O_2]_t)$. As shown in figure 2b, the coefficient $\Delta\phi$ exhibits the typical sigmoidal shape of ligand binding assays for increasing H₂O₂ concentration and can be fitted with the 4-parameter logistic model²⁷. The calibration experiment starts with a partially reduced cyt *c* sample stabilized in 4-(2-hydroxyethyl)-1-piperazineethanesulfonic acid (HEPES) solution, then the value of ϕ decreases with H₂O₂ concentration over a broad dynamic range from 10 pM to 1 μM. The calculated limit of detection, defined as 3-folds the standard deviation of the blank, is below 100 pM of H₂O₂ which is, to our knowledge, at least one order of magnitude lower than described in the literature for biosensors^{6,10}.

Biosensing the H₂O₂ production by stressed aquatic cells. This low limit of detection and extended dynamic range make this method promising for real-time measurements of H₂O₂ traces produced by

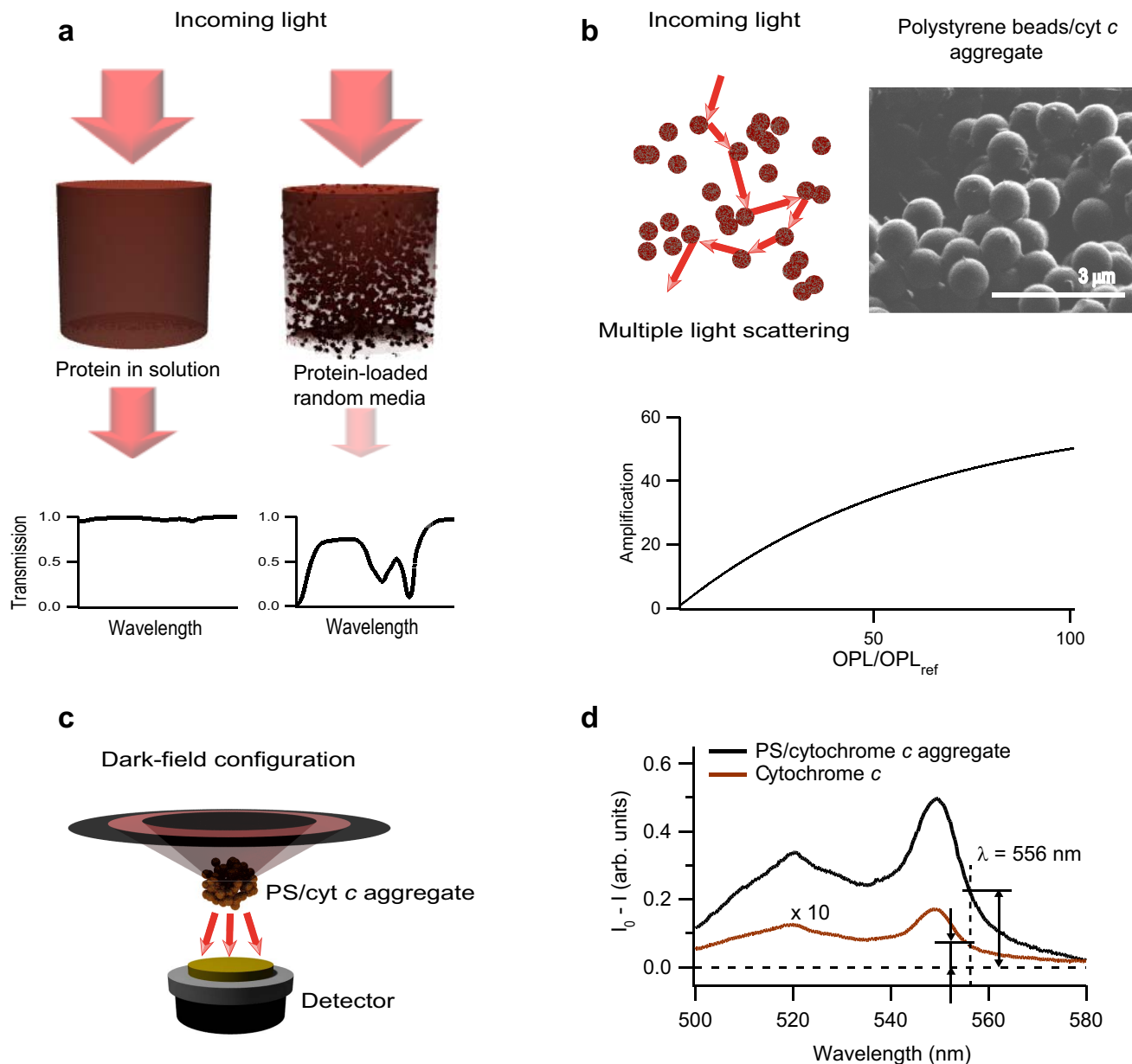


Figure 1 | Method. (a) Schematic illustration of the absorption signal enhancement using multiple scattering in a random medium. Light travelling through a solution containing the absorbing protein exhibits a barely visible signal (left panel), whereas light travelling through a random medium loaded with the same amount of absorbing protein exhibits a large signal due to multiple scattering (right panel). (b) The porous aggregate made of polystyrene beads and cyt *c* (PS/cyt *c*) produces multiple scattering and, consequently, enhances the OIL. The inset shows a micrograph of a PS/cyt *c* aggregate recorded using focused ion beam microscopy. The OIL amplification produced by the random medium is shown in the bottom panel where OIL and OIL_{ref} represent the optical interaction length through a sample with and without PS beads, respectively (see panel (a) and Supplementary Information). (c) Schematic of the experimental setup. The measurements are carried out using an inverted microscope in dark-field configuration connected to a monochromator and CCD camera. (d) Comparison of the cyt *c* absorption measured with (solid black line) and without (solid red line, multiplied 10×) a scattering medium. The number of cyt *c* in the optical path is kept constant for both measurements.

living cells. Here, to obtain dynamic information on cell oxidative status changes, we measured in real-time the amount of H₂O₂ released in a suspension of *C. reinhardtii* (2×10^6 cell ml⁻¹) exposed to 10 and 50 nM of Cd(II), as well as unexposed controls, over a period of 300 min (Fig. 3). In the absence of Cd(II), the H₂O₂ production inherent to the physiological activity of *C. reinhardtii* reached 3×10^4 molecule cell⁻¹ (Fig. 3c). Similarly to absorbance-based assays in which raw optical densities are corrected from initial values and treated as $\Delta A = |A_t - A_0|$, the evolution of the oxidation state coefficient is here expressed as $\Delta\phi = |\phi_t - \phi_0|$. The variation of the oxidation state coefficient, $\Delta\phi$, over time revealed an

overproduction of H₂O₂ in *C. reinhardtii* exposed to 10 and 50 nM of Cd(II) with respect to the non-exposed cells (Fig. 3b). Data obtained in the absence and in the presence of 10 nM of Cd(II) are noisier as compared to those determined in the presence of 50 nM of Cd(II). This is probably due to the flagellar movement of the phytoplanktonic cells during the experiment which leads to temporal fluctuations in the light intensity. However, we observed that the mobility of the cells was seriously affected in the presence of 50 nM of cadmium in the sensing chamber and consequently the signal noise dropped down significantly. The total amount of H₂O₂ production over the 300 min period, obtained from the conversion

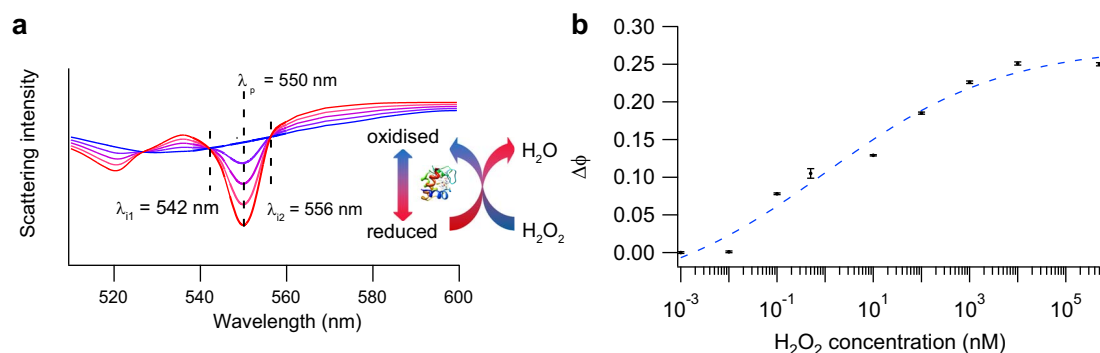


Figure 2 | Spectra and calibration. (a) Reduced and oxidised cyt *c* exhibit different absorption spectra corresponding to the red and blue line, respectively. Upon oxidation of reduced cyt *c* the magnitude of the strong absorption peak at $\lambda_p = 550$ nm decreases, indicating the change of the average oxidation state for the cyt *c* present in the PS aggregate. On the other hand the magnitudes at λ_1 and λ_2 , the intersection points of the spectra of reduced and oxidised cyt *c*, are not affected by a change of the oxidation state and can be used as reference wavelengths for the determination of an oxidation state coefficient ϕ (see Supplementary Information). (b) Calibration curve showing the variation of the oxidation state coefficient $\Delta\phi = \phi_0 - \phi_{[H_2O_2]}$ as a function of the H_2O_2 concentration, where ϕ_0 is the initial coefficient before adding H_2O_2 . Prior to addition of known amounts of H_2O_2 , the cyt *c* has been reduced using ascorbic acid. In the present configuration, the limit-of-detection is lower than 100 pM of H_2O_2 .

of $\Delta\phi$ values into concentration using a calibration curve (see SI), is 10^5 , respectively, 10^8 molecules of H_2O_2 per algal cell exposed to 10, respectively 50 nM of Cd(II). The H_2O_2 production increase per algal cell with Cd(II) concentration in the exposure medium is

consistent with the increase of intracellular Cd content^{23,28}. Similar incidence of sub-lethal Cd(II) concentrations on either the intracellular ROS production or gene expression levels has already been observed after 2.5 and 2 hours exposition time, respectively²⁵.

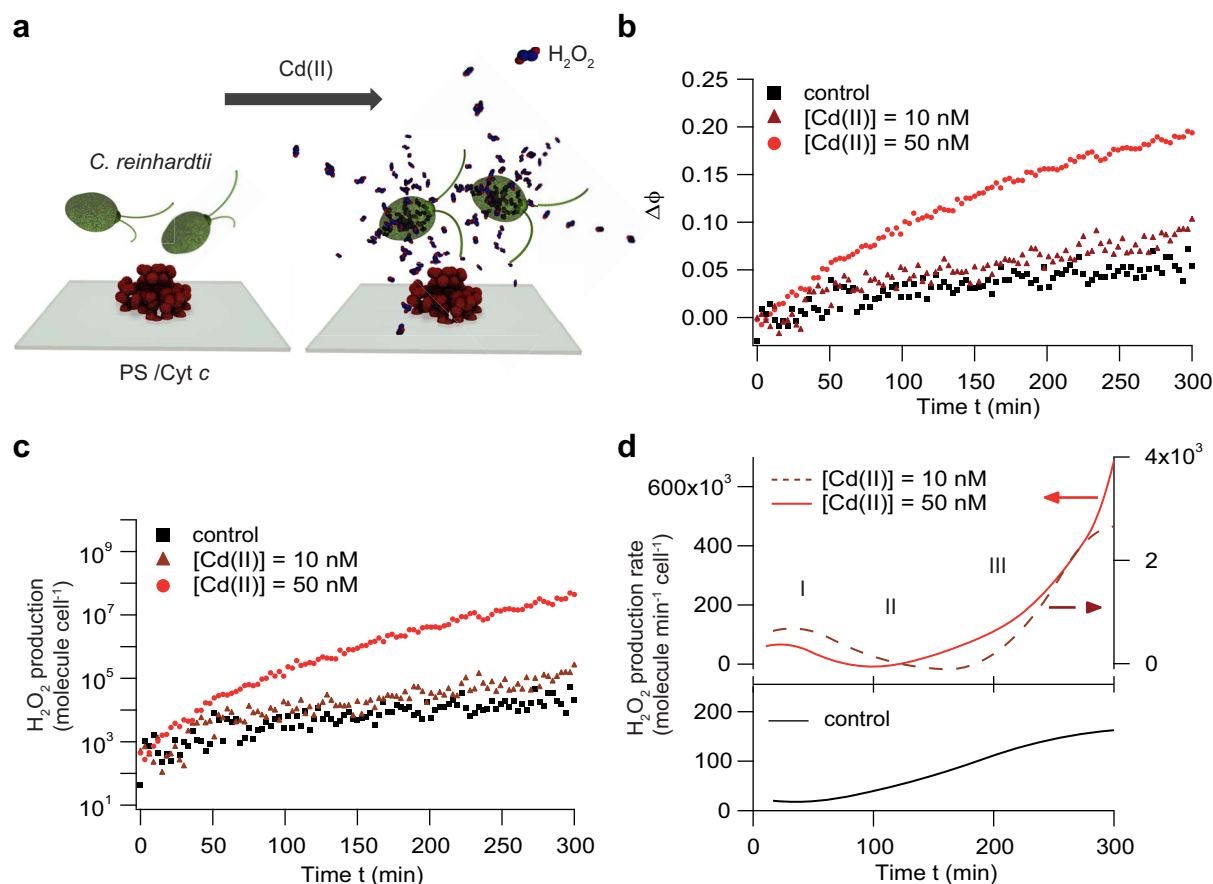


Figure 3 | *C. reinhardtii* exposed to Cd(II). (a) Schematic representation of the real-time detection of H_2O_2 excreted by *C. reinhardtii* (2×10^6 cell ml^{-1} in 1 mM HEPES buffer pH 7.4) exposed to 10 nM, respectively 50 nM, of Cd(II) injected at $t = 0$. Additionally, control experiments are performed without Cd(II) injection. (b) Time evolution of the normalized oxidative state coefficient $\Delta\phi = \phi_0 - \phi_t$ calculated from the raw dark-field spectra using the data treatment (Supplementary Fig. 2). (c) Evolution of the H_2O_2 production (molecule $cell^{-1}$) obtained by converting $\Delta\phi$ values into H_2O_2 concentrations via the calibration curve. (d) Evolution of the H_2O_2 production rate (molecule $min^{-1} cell^{-1}$) calculated from the H_2O_2 production profiles in (c). The upper graph represents the Cd(II)-induced H_2O_2 overproduction rate obtained after subtraction of the control values (lower graph). The following metabolic sequence can be observed: adaptative period (phase I), up-regulation of antioxidants (phase II), and bursting out (phase III).



Corresponding control measurements performed without *C. reinhardtii* revealed that *cyt c* oxidation by Cd(II) and HEPES was negligible over the whole time span of the experiment. These findings agree with the general belief that the Cd(II) toxicity mechanisms are associated with the generation of ROS and demonstrate the capabilities of the proposed new biosensor to obtain quantitative information and, thus, further insights into the dynamics of Cd(II) toxicity mechanisms.

Determination of H₂O₂ production rate. Furthermore, real-time detection gives access to the production rate of H₂O₂ in algae exposed to Cd(II) and can further improve our understanding of the corresponding kinetics. The control experiment in the absence of Cd(II) revealed that the H₂O₂ production rate by *C. reinhardtii* increased progressively from 20 to 150 molecule min⁻¹ cell⁻¹ after a lag period on the order of 40 min (Fig. 3d). Using the typical chlorophyll content in *C. reinhardtii*²² (2.2×10^{-9} (mg Chl) cell⁻¹) we can estimate the H₂O₂ production rate of a few units of pmol H₂O₂ (mg Chl)⁻¹ h⁻¹. Addition of 10 and 50 nM Cd(II) to algal suspensions results in more complex H₂O₂ production rate profiles, as illustrated in figure 3d. The initial plateau in the interval from $t = 20$ to $t = 40$ min corresponding to 7×10^2 and 7×10^4 molecule min⁻¹ cell⁻¹ for 10 and 50 nM Cd(II), respectively, is followed by a gradual decrease of the production rates. A minimum is observed at 110 and 160 min for algae exposed to 10 and 50 nM of Cd(II), respectively. A longer exposure time results in a sharp increase of the production rates, reaching 2.6×10^3 and 7×10^5 molecule min⁻¹ cell⁻¹ after 300 min exposure (Fig. 3d). The observed evolution of the H₂O₂ production rate suggests that, after an adaptive period (phase I, Fig. 3d) which depends on the Cd(II) concentration, antioxidant levels can balance efficiently the accumulation of the ROS within the cell (phase II). Indeed up-regulation of intracellular antioxidant glutathione levels in *C. reinhardtii* after exposure to 80 nM of Cd(II) was observed for a comparable exposure time²⁹. Our data agree also with proteomic studies showing up-regulation of antioxidant proteins such as L-ascorbate peroxidase or superoxide dismutase in *C. reinhardtii* once exposed to 150 μM of Cd(II)³⁰. However, figure 3d shows that this period is then followed by a further increase of the H₂O₂ production rate, suggesting that over a prolonged exposure the antioxidant system is incapable of balancing the excessive ROS production in the cell (phase III). Indeed, the differential transcription of a number of genes involved in oxidative stress defense mechanisms in *C. reinhardtii* exposed to micromolar Cd(II) concentrations after 48 h pointed to an excessive production of ROS⁷. However, this genomic study was performed at much longer exposure times and about 400 to 1000 higher Cd(II) concentrations.

Role of photosynthetic activity on Cd(II)-induced H₂O₂ production. Next, we use this method to examine the dynamics of H₂O₂ production under Cd(II) exposure under different light irradiance conditions. It is known that ROS released inside photosynthetic organisms generally originate from the photosystems II and I (PSII and PSI)^{31,32} located in the thylakoid membrane of the chloroplast where O₂ is reduced to O₂⁻. This transformation is at the beginning of a reaction cascade that leads to the formation of H₂O₂ and hydroxyl radicals •OH. The light driven water splitting reaction in PSII provides dioxygen O₂ whose one-electron reduction is needed to initiate the reaction cascade³³. Previous studies carried out on *C. reinhardtii* have shown that the chloroplasts are readily accessible to Cd(II)³⁴ and the latter causes disorders on both the electron donor and acceptor sides of PSII, leading to the disruption of the photosynthetic chain³⁵. Moreover, it has been recently demonstrated that despite the stromatic antioxidant system, chloroplast-derived H₂O₂ is able to diffuse, most likely through aquaporins, out of chloroplasts³⁶. In the experiment reported in figure 4a *C. reinhardtii* was exposed to 100 nM of Cd(II) at $t = 0$ and

maintained under either light or quasi-dark conditions while monitoring the oxidative state coefficient $\Delta\phi$. Under light conditions the algae are exposed to the light from the source of the microscope whereas under quasi-dark conditions the light, again from the light source of the microscope, is on for only 7 s per min in order to record the *cyt c* absorption spectrum. Clearly, the lack of illumination induces a delay of about 3 h in the overproduction of H₂O₂ in response to Cd(II) exposure, as shown by the corresponding H₂O₂ production curves (Fig. 4b). The analysis of the H₂O₂ production rates (Fig. 4c) stresses a similar time-lag between light and quasi-dark situations, with a rate of 10⁸ molecule min⁻¹ cell⁻¹ reached at $t = 120$ and $t = 320$ min, respectively. The succession of quasi-dark and light periods during the experiment provides further evidence of the impact of Cd(II) on the photosynthetic apparatus (Fig. 4d). The time constants $\tau = 25$ (I), 14 (II), 100 (III) and 14 min⁻¹ (IV), calculated for the corresponding periods defined in figure 4d clearly illustrate that the overproduced H₂O₂ is correlated with the light driven electron extraction from the oxygen evolving complex which is known to remain functional at submicromolar Cd(II) concentrations²⁴. As sketched in figure 4e, it is likely that the overproduction of light-dependent H₂O₂ originates at the PSII acceptor side, as a consequence of disturbed electron transport from PSII towards PSI by Cd(II) binding to the plastoquinone pool³⁷.

Discussion

This biosensing method based on the absorption enhancement of *cyt c* loaded into a random medium enables the development of an ultrasensitive H₂O₂ detection tool. The optical characterization of the PS/*cyt c* aggregate indicates that the extended OIL caused by multiple scattering throughout the random medium produces the amplification of the measured absorption. Hence, minute changes in the *cyt c* spectroscopic response caused by H₂O₂ produced by living cells can be recorded in real-time. Additionally, the data treatment procedure enables the extraction of a normalized redox state coefficient ϕ from raw spectra, which provides quantitative data that are not affected by background variations. The time-evolution of ϕ describes the variations of H₂O₂ concentration during the experiment. This detection method is particularly suitable to study cellular oxidative stress since it is non-invasive and gives access to the H₂O₂ production dynamics in real time. Those operational features represent a considerable advantage over existing end-point techniques based on intracellular ROS detection and open the door to the study of a multitude of physiological mechanisms, ranging from cell signalling to cytotoxicity response. Here, we were able to observe a direct link between Cd(II) toxicity and lighting conditions for an aquatic microorganism. Considering the physical nature of the absorption enhancement, it can be expected that the integration of a bioassay component into a random medium would considerably improve its analytical performances: the method described here to enhance the optical absorption of *cyt c* can be used for other optical systems, such as fluorophores for example. Finally, since numerous enzymatically-catalysed reactions generate H₂O₂ as a by-product, their combination with the novel biosensor proposed in this work would lead to the development of very versatile sensing platforms.

Methods

Optical setup. The spectral measurements are carried out in transmission mode using an inverted microscope (IX71, Olympus) coupled to a monochromator (TRIAX 550, Horiba Scientific) and a CCD camera (Symphony, Horiba Scientific). In all the experiments a 20× objective with NA = 0.35 is used. A 12 V 110 W halogen lamp is used for illumination in a dark field (DF) configuration (DF condenser NA = 0.8/0.92). The light intensity is controlled using the power unit TH4-200 (Olympus). Additionally, low-pass filters attenuating the light with wavelengths above 700 nm are introduced in the illumination path to avoid heating caused by radiation in the infrared. The total light power measured at the output of the DF condenser is 0.5 μW which corresponds to approximately 10 nW absorbed by *cyt c* in the aggregate. The power of light scattered back from the PS aggregate into the measurement chamber

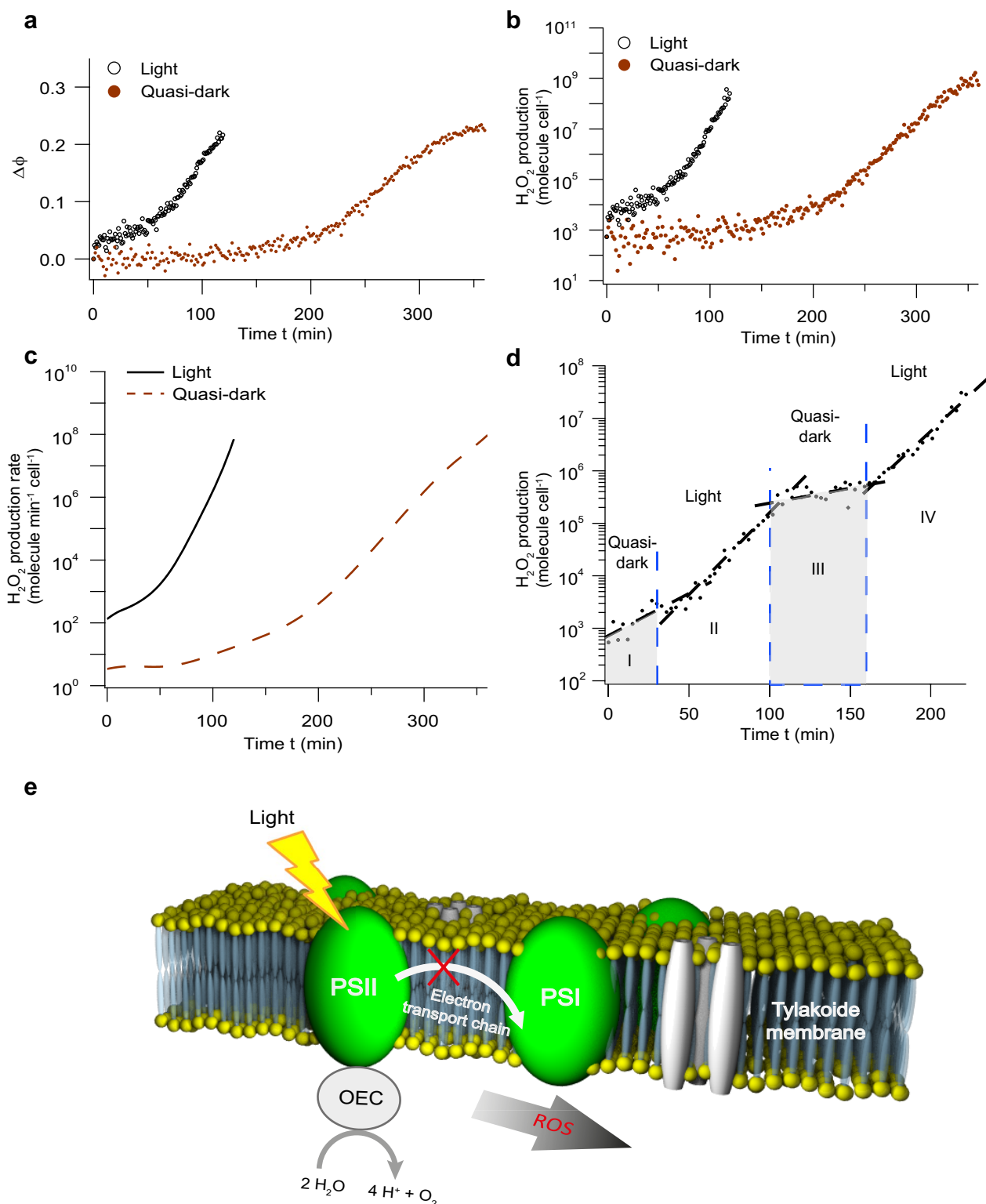


Figure 4 | H_2O_2 production rate under different light conditions. Dark- and light-adapted *C. reinhardtii* (2×10^6 cell ml^{-1} in 1 mM HEPES buffer pH 7.4) are exposed to 100 nM of Cd(II) injected at $t = 0$. The dark-, respectively light-adapted *C. reinhardtii* have been kept in the dark for 12 hours, respectively permanently illuminated. During the experiments, the light-, respectively dark-adapted *C. reinhardtii* are kept under constant illumination, respectively quasi-dark conditions. Under quasi-dark conditions the algae are only illuminated every 3 minutes during 20 s in order to record the spectrum. Time evolution of (a) the oxidation state coefficient $\Delta\phi$, (b) the H_2O_2 production and (c) production rate. After injection of Cd(II) the light-adapted algae under illumination start excreting H_2O_2 without delay, whereas there is a production delay of about 3 h for the dark-adapted algae under quasi-dark conditions. (d) ROS production for dark-adapted algae exposed to 100 nM of Cd(II) when the illumination is successively turned on and off during the measurement. A correlation between illumination and ROS production is clearly visible, with a stronger production under light conditions. The time constants τ associated with the production rate for the different lighting intervals are $\tau(I) = 25 \text{ min}^{-1}$, $\tau(II) = 14 \text{ min}^{-1}$, $\tau(III) = 100 \text{ min}^{-1}$ and $\tau(IV) = 14 \text{ min}^{-1}$. (e) These data support the following action mechanism of Cd(II) on the photosynthetic apparatus of *C. reinhardtii*: Cd(II) binding to the plastoquinone pool disturbs the electron transport chain between PSII and PSI. Upstream, the light driven electron extraction from oxygen evolving complex (OEC) remains functional and generates light-dependent ROS at the PSII acceptor side.



can be estimated lower than 5% of the illumination power. All the measurements have been performed at room temperature between 22 and 25°C.

Preparation of cyt c/PS aggregates. 50 µL of a suspension of polystyrene beads (0.94 µm; Bangs Laboratories) were added into an Eppendorf containing 200 µL of cyt c (200 µM; PBS). The mixture was vortexed for 1 min and 0.5 µL of glutaraldehyde (25%; Sigma-Aldrich) was added to initiate chemical cross-linking. After 30 min the reaction mixture was centrifuged (7800 rpm for 2 min) and after removal of the supernatant, the PS/cyt c aggregates formed were re-suspended into HEPES buffer (1 mM; pH 7.4). This operation was repeated 3 times and the aggregates were stored in HEPES at 4°C.

Determination of amount of cyt c in a PS/cyt c aggregate. In order to determine the amount of cyt c embedded into the PS matrix, the non-reacted cyt c that remained in the supernatant was analyzed by spectrophotometry (at 542 and 556 nm). Absorbance measurements revealed that 5% (2 nmol) of the cyt c initially added into the reaction mixture was retained in the aggregates. For a single aggregate the amount of cyt c was calculated by comparing its mass (dried) to the total mass of the aggregates. It was found that the average cyt c content of each single aggregate was 20 pmol.

Determination of absorption enhancement factor. In order to determine the enhancement of the absorption due to multiple scattering, the same amount of cyt c (20 pmol) present in the PS/cyt c aggregate was placed in the light cone volume (10 µL) by introducing a 2 µM cyt c solution in the measurement chamber. Thus, the comparison of the absorption signals measured in the serial (cyt c solution + separated scatterer) and the parallel (combined cyt c/PS aggregate) configurations, with the same amount of cyt c, provides direct information on the absorption enhancement factor.

Calibration curve. The biosensor response to increasing concentrations of H₂O₂ shown in figure 2b was measured by adding sequentially 0.6 µL of freshly prepared H₂O₂ solutions (from 1 nM to 1 mM) into the sensing chamber containing 60 µL of HEPES (1 mM; pH 7.4). The variation of the oxidative state coefficient, Δφ, corresponding to a given increase in the H₂O₂ concentration, was calculated as the average of five spectral measurements obtained once the equilibrium is reached after 30 minutes. The temperature is kept constant throughout an entire experiment.

Cell culture conditions. The wildtype unicellular freshwater algae *C. reinhardtii* (strain 11 from CPCC, Canadian Phycological Culture Center, Waterloo, ON, Canada) were cultured in diluted Tris-Acetate-Phosphate liquid medium (TAP) under axenic conditions. Cells were grown using a 12 h light/12 h dark regime at 20°C (150 rpm rotary shaking, Rumed incubator, Germany). At the mid-exponential growth phase, cells were harvested by centrifugation (2000× g, 5 min), rinsed with and transferred to 1 mM HEPES. Cell numbers were determined by a Coulter Multisizer III particle counter (Beckman-Coulter, Switzerland) for each experimental run.

Reagents and glassware. Chemicals were provided by Sigma-Aldrich (St. Louis, USA) if not stated otherwise. All glassware and plastic flasks were treated with 10% HNO₃ and rinsed with MilliQ water (18.2 Mohm, Q-H₂O grade) prior to use.

- Finkel, T. & Holbrook, N. J. Oxidants, oxidative stress and the biology of ageing. *Nature* **408**, 239–247 (2000).
- Apel, K. & Hirt, H. Reactive oxygen species: Metabolism, oxidative stress, and signal transduction. *Annu. Rev. Plant Biol.* **55**, 373–399 (2004).
- Sarsour, E. H., Kumar, M. G., Chaudhuri, L., Kalen, A. L. & Goswami, P. C. Redox Control of the Cell Cycle in Health and Disease. *Antioxid. Redox Signal.* **11**, 2985–3011 (2009).
- Vranova, E., Inze, D. & Van Breusegem, F. Signal transduction during oxidative stress. *J. Exp. Bot.* **53**, 1227–1236 (2002).
- Maynard, A. D. *et al.* Safe handling of nanotechnology. *Nature* **444**, 267–269 (2006).
- Casanova, D. *et al.* Single europium-doped nanoparticles measure temporal pattern of reactive oxygen species production inside cells. *Nature Nanotechnology* **4**, 581–585 (2009).
- Jamers, A., Blust, R., De Coen, W., Griffin, J. L. & Jones, O. A. H. An omics based assessment of cadmium toxicity in the green alga *Chlamydomonas reinhardtii*. *Aquat. Toxicol.* **126**, 355–364 (2013).
- Finkelstein, E., Rosen, G. M. & Rauckman, E. J. Spin trapping - Kinetics of the reaction of superoxide and hydroxyl radicals with nitrones. *J. Am. Chem. Soc.* **102**, 4994–4999 (1980).
- Wightman, R. M. Probing cellular chemistry in biological systems with microelectrodes. *Science* **311**, 1570–1574 (2006).
- Jin, H. *et al.* Detection of single-molecule H₂O₂ signalling from epidermal growth factor receptor using fluorescent single-walled carbon nanotubes. *Nature Nanotechnology* **5**, 302–U381 (2010).
- Bohren, C. F. *Clouds in a Glass of Beer*. (John Wiley & Sons, Inc., New York, 1987).
- Wiersma, D. S. The physics and applications of random lasers. *Nature Physics* **4**, 359–367 (2008).

- Muskens, O. L., Rivas, J. G., Algra, R. E., Bakkers, E. & Legendijk, A. Design of light scattering in nanowire materials for photovoltaic applications. *Nano Lett.* **8**, 2638–2642 (2008).
- Svensson, T., Adolffsson, E., Lewander, M., Xu, C. T. & Svanberg, S. Disordered, strongly scattering porous materials as miniature multipass gas cells. *Physical Review Letters* **107** (2011).
- Boustany, N. N., Boppart, S. A. & Backman, V. in *Annual Review of Biomedical Engineering*, Vol 12 Vol. 12 *Annual Review of Biomedical Engineering* (eds Yarmush, M. L., Duncan, J. S. & Gray, M. L.) 285–314 (2010).
- Borghese, F., Denti, P., Toscano, G. & Sindoni, O. I. Electromagnetic scattering by a cluster of spheres. *Appl. Opt.* **18**, 116–120 (1979).
- Ishimaru, A. Wave-Propagation and Scattering in Random-Media and Rough Surfaces. *Proceedings of the IEEE* **79**, 1359–1366 (1991).
- Kim, A. D. in *Nonimaging Optics and Efficient Illumination Systems* Vol. 5529 *Proceedings of the Society of Photo-Optical Instrumentation Engineers (Spie)* (eds R. Winston & R. J. Koschel) 79–86 (Society of Photo Optical, 2004).
- Svensson, T. *et al.* Holey random walks: Optics of heterogeneous turbid composites. *Physical Review E* **87** (2013).
- Grossman, A. R. In the grip of algal genomics. *Adv. Exp. Med. Biol.* **616**, 54–76 (2007).
- Suárez, C., Torres, E., Pérez-Rama, M., Herrero, C. & Abalde, J. Cadmium toxicity on the freshwater microalga *Chlamydomonas moewusii* Gerloff: Biosynthesis of thiol compounds. *Environ. Toxicol. Chem.* **29**, 2009–2015 (2010).
- Kosourov, S., Tsygankov, A., Seibert, M. & Ghirardi, M. L. Sustained hydrogen photoproduction by *Chlamydomonas reinhardtii*: Effects of culture parameters. *Biotechnol. Bioeng.* **78**, 731–740 (2002).
- Simon, D. F., Descombes, P., Zerges, W. & Wilkinson, K. J. Global expression profiling of *Chlamydomonas reinhardtii* exposed to trace levels of free cadmium. *Environ. Toxicol. Chem.* **27**, 1668–1675 (2008).
- Szivaik, I., Behra, R. & Sigg, L. Metal-induced reactive oxygen species production in *Chlamydomonas reinhardtii* (chlorophyceae). *J. Phycol.* **45**, 427–435 (2009).
- Hanikenne, M. *Chlamydomonas reinhardtii* as a eukaryotic photosynthetic model for studies of heavy metal homeostasis and tolerance. *New Phytol.* **159**, 331–340 (2003).
- Tessier, A. & Turner, D. *Metal Speciation and Bioavailability in Aquatic Systems*. (John Wiley & Sons, 1995).
- Findlay, J. W. A. & Dillard, R. F. Appropriate calibration curve fitting in ligand binding assays. *AAPS Journal* **9**, E260–E267 (2007).
- Kola, H. & Wilkinson, K. J. Cadmium uptake by a green alga can be predicted by equilibrium modelling. *Environmental Science and Technology* **39**, 3040–3047 (2005).
- Stoiber, T. L., Shafer, M. M. & Armstrong, D. E. Differential effects of copper and cadmium exposure on toxicity endpoints and gene expression in *Chlamydomonas reinhardtii*. *Environ. Toxicol. Chem.* **29**, 191–200 (2010).
- Gillet, S., Decottignies, P., Chardonnet, S. & Le Marechal, P. Cadmium response and redoxin targets in *Chlamydomonas reinhardtii*: a proteomic approach. *Photosynthesis Res.* **89**, 201–211 (2006).
- Asada, K. Production and scavenging of reactive oxygen species in chloroplasts and their functions. *Plant Physiol.* **141**, 391–396 (2006).
- Pospisil, P. Production of reactive oxygen species by photosystem II. *Biochimica Et Biophysica Acta-Bioenergetics* **1787**, 1151–1160 (2009).
- Barber, J. Photosynthetic energy conversion: natural and artificial. *Chemical Society Reviews* **38**, 185–196 (2009).
- Nagel, K., Adelmeier, U. & Voigt, J. Subcellular distribution of cadmium in the unicellular green alga *Chlamydomonas reinhardtii*. *J. Plant Physiol.* **149**, 86–90 (1996).
- Faller, P., Kienzler, K. & Krieger-Liszka, A. Mechanism of Cd²⁺ toxicity: Cd²⁺ inhibits photoactivation of Photosystem II by competitive binding to the essential Ca²⁺ site. *Biochimica Et Biophysica Acta-Bioenergetics* **1706**, 158–164 (2005).
- Mubarakshina, M. M. & Ivanov, B. N. The production and scavenging of reactive oxygen species in the plastoquinone pool of chloroplast thylakoid membranes. *Physiol. Plant.* **140**, 103–110 (2010).
- Sigfridsson, K. G. V., Bernat, G., Mamedov, F. & Styring, S. Molecular interference of Cd²⁺ with Photosystem II. *Biochimica Et Biophysica Acta-Bioenergetics* **1659**, 19–31 (2004).

Acknowledgments

This work was supported by the Swiss National Science Foundation (projects CR2312_130164 and 406440_131280 in the framework of the Swiss National Research Program NRP 64).

Author contributions

G.S., C.S., V.I.S. and O.J.F.M. contributed to the data analysis and the manuscript writing; G.S., C.S. and O.J.F.M. designed the experiment; G.S. and C.S. performed the measurements; G.S. and V.I.S. cultured the cells.

Additional information

Supplementary information accompanies this paper at <http://www.nature.com/scientificreports>



Competing financial interests: The authors declare no competing financial interests.

How to cite this article: Suárez, G., Santschi, C., Slaveykova, V.I. & Martin, O.J.F. Sensing the dynamics of oxidative stress using enhanced absorption in protein-loaded random media. *Sci. Rep.* 3, 3447; DOI:10.1038/srep03447 (2013).



This work is licensed under a Creative Commons Attribution-NonCommercial-ShareAlike 3.0 Unported license. To view a copy of this license, visit <http://creativecommons.org/licenses/by-nc-sa/3.0>